High Efficiency Resonant DC/DC Converter Utilizing a Resistance Compression Network

Citation: Inam, Wardah, Khurram K. Afridi, and David J. Perreault. "High Efficiency Resonant DC/DC Converter Utilizing a Resistance Compression Network." IEEE Trans. Power Electron. 29, no. 8 (n.d.): 4126–4135.

As Published: http://dx.doi.org/10.1109/TPEL.2013.2282626

Publisher: Institute of Electrical and Electronics Engineers (IEEE)

Persistent URL: http://hdl.handle.net/1721.1/87094

Version: Author's final manuscript: final author's manuscript post peer review, without publisher's formatting or copy editing

High Efficiency Resonant dc/dc Converter Utilizing a Resistance Compression Network

Wardah Inam, *Student Member, IEEE*, Khurram K. Afridi, *Member, IEEE*, and David J. Perreault, *Fellow, IEEE*

***Abstract*— This paper presents a new topology for a high efficiency dc/dc resonant power converter that utilizes a resistance compression network to provide simultaneous zero voltage switching and near zero current switching across a wide range of input voltage, output voltage and power levels. The resistance compression network (RCN) maintains desired current waveforms over a wide range of voltage operating conditions. The use of on/off control in conjunction with narrowband frequency control enables high efficiency to be maintained across a wide range of power levels. The converter implementation provides galvanic isolation and enables large (greater than 1:10) voltage conversion ratios, making the system suitable for large step-up conversion in applications such as distributed photovoltaic converters. Experimental results from a 200 W prototype operating at 500 kHz show that over 95% efficiency is maintained across an input voltage range of 25 V to 40 V with an output voltage of 400 V. It is also shown that the converter operates very efficiently over a wide output voltage range of 250 V to 400 V, and a wide output power range of 20 W to 200 W. These experimental results demonstrate the effectiveness of the proposed design.**

***Index Terms*- dc/dc converter, resonant converter, on-off control, high efficiency power converter, resistance compression network**

I. Introduction

High-voltage-gain dc/dc converters are found in a variety of applications [1]- [4]. For example, to connect photovoltaic panels to the grid, interface circuitry is needed. Some architectures for this purpose incorporate dc/dc converters to boost voltage of individual photovoltaic panels to a high dc-link voltage, with follow-on electronics for converting dc to ac (e.g., [5], [6]). The step-up dc/dc converter is a critical part of this system, and must operate efficiently for a large voltage step-up and for a wide voltage range (e.g., at the converter input and/or output depending upon the system). Furthermore, to be compact it must operate at high switching frequencies.

In conventional hard-switched power converters, the overlap of current and voltage is large during switching, resulting in significant power loss, especially at high frequencies. Soft switched resonant converter topologies providing zero voltage switching (ZVS) or zero current switching (ZCS) can greatly reduce loss at the switching transitions, enabling high efficiency at high frequencies (e.g., [7], [8]). Unfortunately, while many soft-switched resonant designs achieve excellent performance for nominal operating conditions, performance can degrade quickly with variation in input and output voltages and power levels [9], [10].

Limitations on the efficient operating range of resonant converters are tied to both converter structure and control. Numerous control techniques are possible for compensating variations in input voltage, output voltage, and power level. These include frequency control [7], [8], phase-shift PWM control [11], asymmetric duty cycle PWM control [12], and on-off or burst mode control [13]. Each of these control techniques in conjunction with conventional resonant tank structures imposes significant design limits. For example, the conventional half-bridge Series Resonant Converter (SRC) [8] requires wide-band frequency variation to control the power when output load or input voltage varies such that the magnetics cannot be optimally designed. Furthermore, to maintain zero-voltage switching the frequency must increase to reduce power, hurting the efficiency at light load. For a full-bridge version of the SRC, phase shift control can be used to control the power and reject conversion ratio variations (e.g., [11]). However, this results in asymmetrical current levels in the switches at the switching instants, with the switches in the leading leg turning off at high currents. The effective impedance of the rectifier in a resonant converter also often causes challenges, as it varies with operating conditions.

This paper introduces a new high efficiency resonant dc/dc converter topology, the Resistance Compression Network (RCN) converter, which seeks to overcome the above-mentioned challenges. This converter operates with simultaneous zero voltage switching (ZVS) and near zero current switching (ZCS) across a wide range of input voltage, output voltage and power levels, resulting in low switching losses. This work represents an expansion on an earlier conference paper [14], and includes additional experimental results and estimates of loss breakdown.

The remainder of this paper is organized as follows: Section II describes the topology and control of the proposed RCN dc/dc converter. The converter is analyzed and methodology for its design is presented in section III. Section IV describes the design and implementation of a prototype RCN dc/dc converter. The experimental results from this prototype are presented and discussed in section V. Finally, section VI summarizes the conclusion of the paper. The equations used to estimate the losses in the various components are given in an Appendix.

II. RCN Converter Topology and Control

The dc/dc converter proposed here consists of an inversion stage, a transformation stage and a rectification stage, as shown in Fig. 1. The inversion and rectification stages use standard designs. However, the transformation stage and the control of the converter are new. The topology of the proposed Resistance Compression Network (RCN) converter is shown in Fig. 2. The converter as shown is designed to step-up voltage. The transformation stage consists of a matching network, a transformer, and a resistance compression network (RCN). The

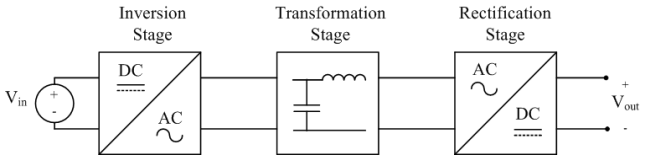

Fig. 1: Architecture of proposed dc/dc converter.

matching network composed of L_{rp} and C_{rp} acts as a filter and provides a voltage gain [17], hence reducing the transformer turns ratio requirement. One issue with high-turns-ratio step-up transformers that exists in many topologies is that the parasitic leakage inductance of the transformer can undesirably ring with its secondary side winding capacitance at the switching transitions. This creates large ringing in the current and voltage waveforms, and high-frequency losses. The matching network also eliminates this ringing by absorbing the transformer parasitics. The 1:N transformer provides additional voltage gain and isolation. The resistance compression network (composed of L_s and C_s) is a special single input, multi-output matching network that provides desirable impedance control characteristics [15], [16], [23]. The RCN technique was originally proposed and applied for radio-frequency (RF) applications, such as very-high-frequency dc/dc converter systems [15] and RF power amplifiers [16]; here we exploit if for high efficiency power conversion. The function of the RCN is to automatically regulate the converter operating power and waveforms in a desirable manner as the input and output voltages vary. As applied here, the RCN also includes a series resonant tank (composed of L_r and C_r) [8]. Its purpose is to provide additional filtering. The inverter stage is simply a full-bridge inverter (composed of switches $S_1 - S_4$). A full-bridge is used instead of a half-bridge to reduce the voltage gain requirement from the matching network and the transformer. The rectification stage is composed of two half-bridge rectifiers. The capacitors C_{in} and C_{out} are for input and output filtering, respectively, and the two capacitors marked as C_{DC} are for dc blocking purposes.

The output power in the proposed converter is regulated using on-off control, also known as burst-mode control or bang-bang control. Power is controlled by gating the converter on and off at a modulation frequency that is much lower than the switching frequency [13], [15], [21]. The advantage of using on-off control is that the magnetics are designed for only a single frequency (a high frequency) while the power is regulated by turning the converter on and off at a lower frequency. Moreover, the power is transferred only in the fraction of the time the converter is on, which results in high efficiency even at light loads. The output power is controlled by the duty ratio of the on-off modulation.On-off control can be implemented through hysteretic control (e.g. [18], [19], [20]), through fixed-period on-off PWM (e.g., [21]), or other methods. Additional care may be necessary in implementations that allow very short on or off durations to maintain high efficiency and desired operation during on-off transient conditions.

The on-off modulation has its own corresponding loss. The higher the modulation frequency the greater the loss. The output capacitance is sized according to the on-off modulation frequency; with a lower modulation frequency a larger capacitor has to be used. The duty ratio of the modulation also influences the loss. Very small or very large duty ratio results in greater loss as the converter operates in steady state for a shorter time. So, in order to minimize the total loss both the modulation frequency and the duty ratio have to be considered.

III. Analysis and Design Methodology

Using fundamental frequency analysis, at the switching frequency the half-bridge rectifiers can be modeled as resistors [8], [16], as illustrated in Fig. 3. The effective resistance of these rectifiers is given by:

$$R_L = \frac{4V_{out}^2}{\pi^2 P_{out}}, \tag{1}$$

where V_{out} is the converter output voltage and P_{out} is the switching-cycle-average output power. As shown in Fig. 2, one of the branches of the RCN comprises a blocking capacitor C_{DC} and an RCN inductor L_s. The other branch comprises a series LC tank tuned to be net capacitive at the switching frequency (net equivalent capacitance C_s). This branch may be modeled as a series resonant tank (with components L_r and C_r) tuned to the switching frequency for filtering, in series with an additional RCN capacitance C_s. Since the series LC tank appears as a short circuit at the switching frequency, it is treated as such in Fig. 3 and in the following analysis. Similarly the dc blocking capacitor C_{DC} of Fig. 2 is an

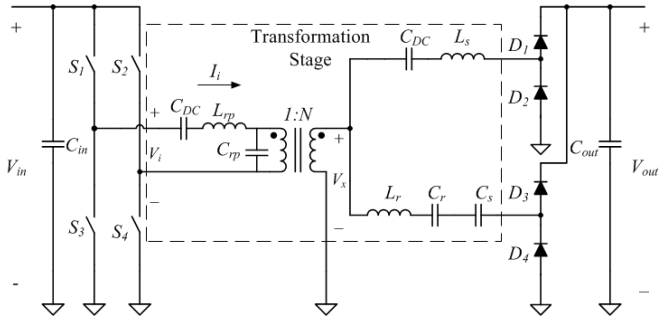

Fig. 2: Topology of the proposed Resistance Compression Network (RCN) dc/dc converter.

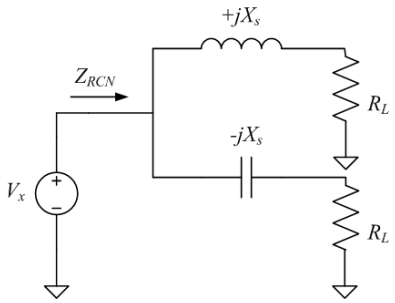

Fig. 3: Fundamental frequency model of the resistance compression network (RCN) and the rectifiers.

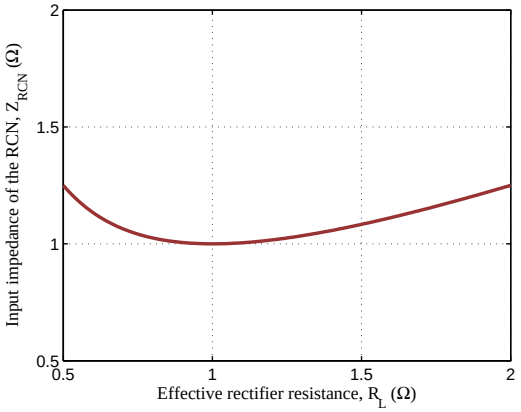

Fig. 4: Variation in the resistive input impedance of the resistance compression network (Z_{RCN}) as a function of the effective rectifier resistance (R_L). Z_{RCN} is plotted assuming the reactance X_s has a value of 1 Ω.

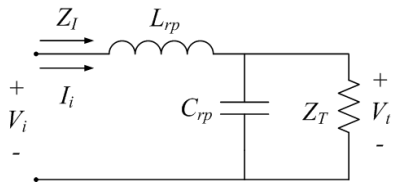

Fig. 5: Matching network with equivalent impedance.

effective short at the high switching frequency. Hence, at the switching frequency the input impedance of the RCN looks purely resistive and is given by:

$$Z_{RCN} = \frac{X_s^2 + R_L^2}{2R_L}, \tag{2}$$

where X_s is the magnitude of impedance of the RCN elements (L_s and C_s) at the switching frequency. The use of the resistance compression network reduces the change in impedance seen by the inverter as the effective rectifier resistance (R_L) changes due to variations in output voltage and output power [15], [16]. This compression effect can be seen in Fig. 4, which shows that the RCN input impedance (Z_{RCN}) varies only by 25% while the effective rectifier resistance varies by 400%. This helps achieve zero voltage switching (ZVS) and near zero current switching (ZCS) of the inverter switches across a wide range of output and input voltages. The RCN also serves to limit the instantaneous output power across the full operating range by providing a specified loading characteristic to the inverter. The value of X_s is selected in such a way so as to limit the output power to the maximum value required across the range of output voltages at the minimum input voltage. Since the power delivery capability of the converter increases with input voltage, this ensures that the converter can deliver the maximum required power across its entire input voltage range. It is also noted that the power characteristic across output voltage is quite flat at the minimum input voltage, owing to the effect of the resistance compression network. The expression for output power (P_{out}) can be found by neglecting losses and equating input power (P_{in}=$(\frac{4}{\pi}V_{in})^2/2Z_I$, where Z_I is the input impedance of the matching network as shown in Fig. 5) to output power (P_{out}=$4V_{out}^2/\pi^2 R_L$). The output power of the converter is given by:

$$P_{out} = \frac{4V_{out}}{X_s\pi^2}\sqrt{4V_{in}^2N^2G^2 - V_{out}^2}. \tag{3}$$

This expression for output power is in terms of input voltage (V_{in}), output voltage (V_{out}), the transformer turns ratio (N) and the matching network gain voltage (G).

The gain of the matching network can be calculated using the equivalent circuit of Fig. 5 and is given by:

$$G \equiv \frac{V_t}{V_i} = \frac{1}{\sqrt{(\frac{\omega L_{rp}}{Z_T})^2 + (1-\omega^2 L_{rp}C_{rp})^2}}, \tag{4}$$

where ω is the angular switching frequency. Here Z_T (=Z_{RCN}/N^2) is the effective load seen by the matching network. As Z_T varies with changes in power, the gain varies. However, due to the resistance compression network, this gain is fairly constant across variation in input and output voltage. The input impedance of the matching network as seen by the inverter is given by:

$$Z_I = \frac{j(X_{Lrp}Z_T^2 + X_{Crp}^2X_{Lrp} - X_{Crp}Z_T^2) + X_{Crp}^2Z_T}{Z_T^2 + X_{Crp}^2}, \tag{5}$$

where X_{Lrp} and X_{Crp} are the magnitude of the impedance of L_{rp} and C_{rp}, respectively. For Z_I to be resistive, X_{Lrp}, X_{Crp} and Z_T must satisfy:

$$X_{Lrp} = \frac{X_{Crp}Z_T^2}{X_{Crp}^2 + Z_T^2}. \tag{6}$$

Picking X_{Lrp} to be slightly larger than the value given by (6), so that Z_I is slightly inductive, ensures that the inverter switches achieve zero voltage switching (ZVS) and near zero current switching (ZCS). The application of the equations presented above is illustrated in the design of the prototype converter in the next section.

IV. Prototype Converter Design

A prototype of the RCN dc/dc converter of Fig. 6 has been designed and built. The designed dc/dc converter is meant for large-step-up applications such as the two-stage photovoltaic-to-grid conversion system shown in Fig. 7. The RCN dc/dc converter can be used to convert the low (widely varying) output voltage of a photovoltaic panel into a high dc-link voltage, for example. The design specifications for this prototype are given in Table I. The converter is required to operate over an input voltage range of 25-40 V, an output voltage range of 250-400 V and over a wide output power range of 20-200 W.

The switching frequency of the converter was selected as 500 kHz. This frequency minimized the total losses in the magnetics (assuming 3F3 magnetic material and RM cores) and the transistors as shown in Fig. 8. Given that the architecture provides relatively low transistor switching losses, selection of a different magnetic material could enable significantly higher

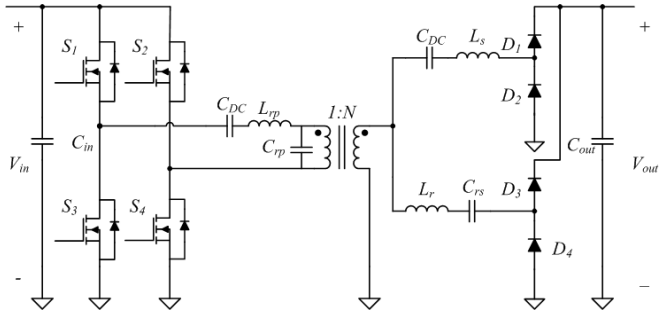

Fig. 6: Implementation of the proposed Resistance Compression Network (RCN) dc/dc converter.

TABLE I: Design Specifications for the Prototype Converter.

Parameter	Value
Input Voltage (V_{in}) Range	25 V - 40 V
Output Voltage (V_{out}) Range	250 V - 400 V
Output Power (P_{out}) Range	20 W - 200 W

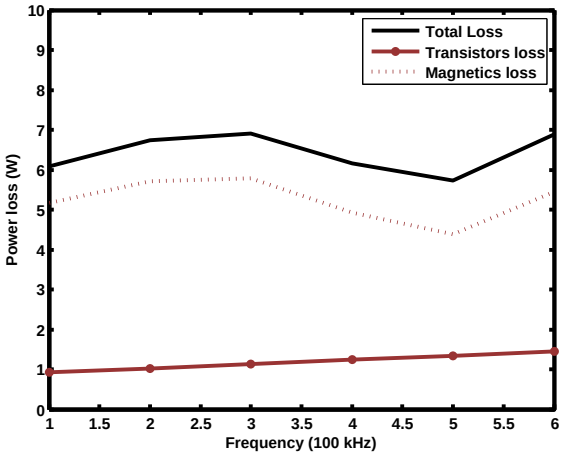

Fig. 8: Loss in the converter in the magnetics and switches when soft-switched and hard-switched at different frequencies.

frequencies to be utilized. The on/off modulation frequency for output power control was chosen as 500 Hz. The reason for selecting this low frequency was to achieve a high efficiency under modulation with acceptable capacitance at the input and output. In applications where capacitance reduction is desired, significantly higher modulation frequencies can be realized. The components used in the inversion, transformation and rectification stage of the converter are listed in Table II. For the full-bridge inverter, EPC 100-V/25-A enhancement mode GaN transistors (EPC2001) were used. Two of these devices were paralleled for each switch to reduce the conduction loss. Two half-bridge gate drivers for enhancement mode GaN FETs (LM5113) were used for transistor drive. The transistors are switched at 500 kHz using TI's digital signal controller (TMS320F28335). This has PWM modules that can easily be programmed to produce the required waveforms with a minimum of 10 ns dead time. For the rectifier, silicon carbide Schottky diodes (C3D02060E) were used. These are 2 A devices with 600 V blocking capability.

For the transformation stage, the reactive elements values were chosen considering the trade-offs between the losses in the parasitics of the transformer, the matching network and the RCN. If the total gain provided by the transformer and matching network is increased, the magnitude of impedance of the RCN also has to be increased. This helps in reducing the increase in output power at higher output voltages, which in turn helps maintain high efficiencies at the higher output voltages. If more gain is provided by the matching network,

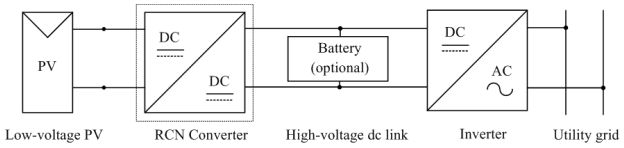

Fig. 7: Block diagram of a grid-connected PV system.

the value of the matching network inductance increases, and thus the matching network loss also increases. However, this results in a decrease in the required gain of the transformer which can result in a decrease in transformer loss.

A trade-off of the losses in the transformer and matching network was considered to determine the value of the gain of these elements. For the matching network, an achievable inductor Q was selected, and the results of [17] were used to compute the loss of the matching network for a range of matching network gain values. Each matching network gain results in a specified transformer gain. A computer search routine was then used to identify the best transformer design for each specified gain. Transformers were designed by searching fully across a set of specified cores and wire/foil configurations to minimize transformer loss (the code provided in [22], which uses the power loss equations given in the appendix, was used to estimate these losses). The split of gains (between matching network and transformer) and the transformer design leading to the lowest total computed loss were then selected. For available cores and wires, the transformer turns ratio (N) was chosen to be 6 and the gain of the matching network (G) was chosen to be 1.67, for a total gain of approximately 10. It is noted that more sophisticated optimizations could yield better results. This could include fully optimizing the design of the matching network inductor as part of the search to co-optimize the transformer/matching-network system (e.g., to maximize the achievable overall efficiency in a given volume). Likewise, introduction of more sophisticated loss models could be expected to provide refined results. Nevertheless, the method utilized is efficient and yields good results.

The value of X_s was calculated using (3) with the output power set to a value of 200 W and input voltage set to its minimum value of 25 V and output voltage set to 400 V. This ensures output power of 200 W across the entire input voltage range. To ensure output power of 200 W across the entire output voltage range the maximum value of X_s needs to be selected with an input voltage set at 25 V, output power at 200 W and varying the output voltage from 250 V to 400 V.

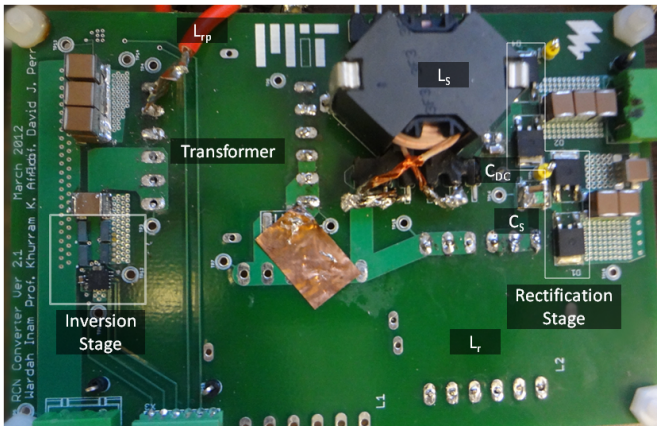

Fig. 9: Photograph of the prototype RCN dc/dc converter (Top side).

The two values are very similar in this case as the resistance compression network greatly reduces the variation in output resistance with change in output voltage. From this the value of L_s and C_s were obtained using L_s=X_s/ω and C_s= $1/\omega X_s$. The values of L_{rp} and C_{rp} were calculated using (4) and (6) which makes the input impedance of the matching network resistive. However, the value of L_{rp} was increased slightly to provide slightly inductive loading of the inverter to achieve ZVS switching of the inverter switches.

For the design of the magnetic structure, a trade-off was made between loss and size. For the transformer and inductors, different core sizes (RM10, RM12 and RM14) and types of windings (litz wire and foil) were considered. For the transformer, RM12 provided a good balance between loss and size. Copper foil was chosen for the primary winding due to the high current (With a maximum peak current of 9.42 A) and litz wire was chosen for the secondary winding to reduce the proximity effect given the large number of turns (with a maximum peak current of 1.57 A). For the inductors (L_s, L_r and L_{rp}), RM12 core and litz wire were chosen. The design value for C_s was 1300 pF and for C_r was 1000 pF. A single mica capacitor C_{rs} of 560 pF was used to provide the correct net capacitance, as shown in Fig. 6. This capacitor had a maximum peak voltage of 795 V with a DC voltage of 200 V. Six 10 nF ceramic capacitors with very low equivalent series resistance (ESR) were used for C_{rp}. These capacitors saw a maximum peak voltage of 65.6 V. Further design details of this converter are given in [22]. A photograph of the top side of the prototype converter is shown in Fig. 9 and the bottom side is shown in Fig. 10.

V. Experimental Results

The prototype RCN dc/dc converter has been tested using a dc power supply and a resistive load. The tests were carried out with different input voltages (in the 25-40 V range) and different output voltages (in the 250-400 V range). Figure 11 shows current and voltage waveforms for the converter over two switching periods, when operated at an input voltage of 25 V. In particular, it shows the current through the inductor of the matching network, which is also the output current of

TABLE II: Components Used in the Experimental Prototype.

Components	Type
Transistors	100-V/25-A GaN enhacemnet mode power transistor (EPC's EPC2001), Qty: 8 (2 in parallel per switch)
Drivers	100-V/5-A half-bridge gate driver for enhancement mode GaN FETs (TI's LM5113), Qty: 2
Controller	150 MHz digital signal controller (TI's TMS320F28335), Qty: 1
Diodes	600-V/2-A SiC Schottky diode (CREE's C3D02060E), Qty: 4
Transformer	RM12 3F3 core, Copper foil (4 turns, 5 mils width, 3 mils thickness, 3 foils in parallel) and litz wire (24 turns, 46 AWG, 450 strands in parallel)
Capacitors	C_{rs}: 560 pF/1000-V Mica capacitor (C_s:1300 pF and C_r:1000 pF) C_{rp}: 60 nF Ceramic capacitors, Qty: 6 (10 nF capacitors in parallel)
Inductors	L_{rp}: 1 μH, RM12A115 3F3 core, litz wire (3 turns, 46AWG, 3600 strands in parallel), L_s: 78 μH, RM12A080 3F3 core, litz wire (31 turns, 46AWG, 450 strands in Parallel), L_r: 101 μH, RM12A060 3F3 core, litz wire (41 turns, 46AWG, 450 strands in parallel)

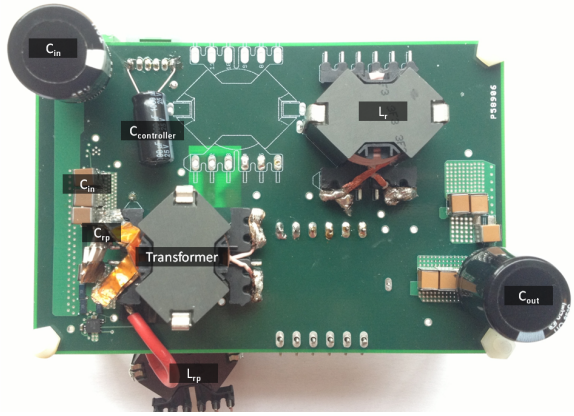

Fig. 10: Photograph of the prototype RCN dc/dc converter (Bottom side).

the inverter, the gate drive voltages of the inverter switches S_1 and S_3, and the drain-source voltage of the switch S_3. As expected, the current through the inductor of the matching network is approximately sinusoidal. Also, the switches achieve zero-voltage switching (ZVS) and near-zero-current switching (ZCS), as can be seen from Fig. 12. Even with the slight distortion in currents that occur owing to limited tank Q, ZVS and near ZCS is still achieved as predicted with sinusoidal approximations. This owes in part to the fact that even with moderate damping of the resonant oscillation owing to the rectifier network, the current waveform still tends towards zero (at a reduced slope) for the next switching transition. Figure 12(a) shows a zoomed in view of the turn-off transition of switch S_3. The current through switch S_3 at turn-off is small compared to both the peak and average of the current it carries (turn-off current is 15.7% of peak current and 27.5% of average current). Figure 12(b) shows the turn-on transition of switch S_3. Notice that the switch turns

on under ZVS, as the voltage across the switch falls to zero before the switch is turned on. Figure 13 shows the current and voltage waveforms with an input voltage of 40 V and an output voltage of 400 V. The converter was operated slightly off resonance at 425 kHz switching frequency to decrease the instantaneous output power at the increased input voltage. This off resonance operation results in a slight distortion of the current waveform as can be seen in Fig. 13. However, the converter still maintains ZVS and near ZCS operation as the input impedance of the matching network still remains slightly inductive. The converter maintains near ZCS operation over the entire input voltage and output voltage range. The highest current at switch turn-off is no more than 13.6% of peak switch current (and 24.4% of average current) when the converter is operated at its nominal input voltage of 32.5 V; and when the input voltage is at its maximum of 40 V, the switch turn-off current rises to only 18.9% of peak switch current (and 50% of average current).

As illustrated above, narrow-range frequency operation is used to improve the overall performance of the converter. By adjusting the converter switching frequency over a narrow range from 425 kHz to 500 kHz as input voltage varies, the maximum output power that can be delivered by the converter can be maintained within a narrower range than if strictly fixed-frequency operation is used, yielding moderate power variation across variations in input voltage. This helps maintain high efficiency as the input voltage varies. The switching frequency is decreased as the input voltage increased: 500 kHz is used at an input voltage of 25 V and 425 kHz with an input voltage of 40 V. The maximum output power then varies from 200 W to 325 W across the full range of input voltage, with the output voltage at 400 V, as shown in Fig. 15(a). The converter can certainly be operating at fixed frequency over the complete input voltage range (for cases where absolute fixed-frequency operation is desired). However, this results in higher instantaneous output power at higher input voltages, as illustrated by the comparison of Fig.14 (operation at fixed frequency) to Fig. 15 (operation with small frequency variation). Figure 16 shows a comparison of the variation in instantaneous output power as a function of input voltage and output voltage at fixed switching frequency versus variable switching frequency). It can be seen that the use of modest frequency variation as the input voltage varies serves to reduce the effect of input voltage variations on converter operation.

The converter was also tested for output voltage variations from 250 V to 400 V. When the output voltage is reduced from 400 V to 250 V with input voltage held at 25 V (and switching frequency correspondingly held constant), the maximum output power varies over only a very narrow range, dropping slightly from 203 W to 195 W, as shown in Fig. 15(b). It can be seen that the RCN is highly effective in suppressing the effects of output voltage variation on the operation (e.g., instantaneous power) of the converter. By using the RCN to greatly limit the effects of output voltage variation, and narrow-range frequency control to moderately reduce the effects of input voltage variation, good performance over wide voltage operating ranges is achieved.

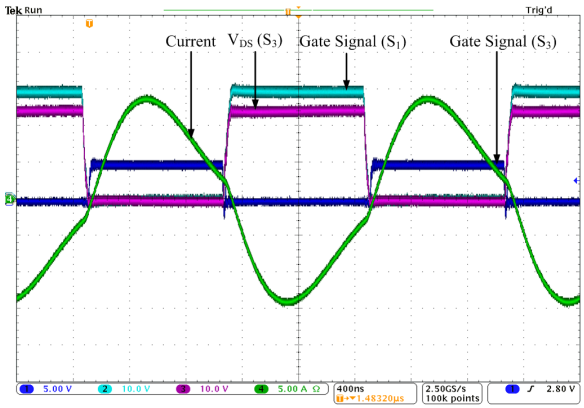

Fig. 11: Current and voltage waveforms of the RCN dc/dc converter when operated at an input voltage of 25 V: (1-blue) Gate voltage of switch S_3, (2-turquise) gate voltage of switch S_1, (3-magenta) drain-source voltage of switch S_3 and (4-green) current through inductor of the matching network.

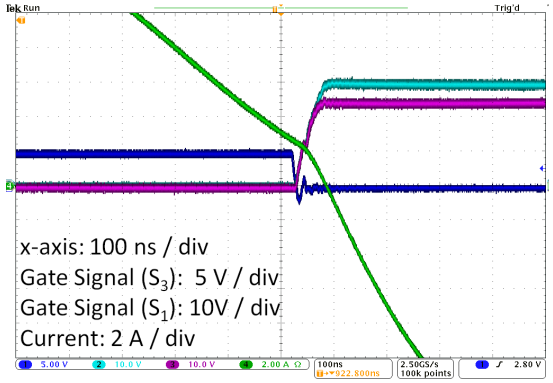

(a)

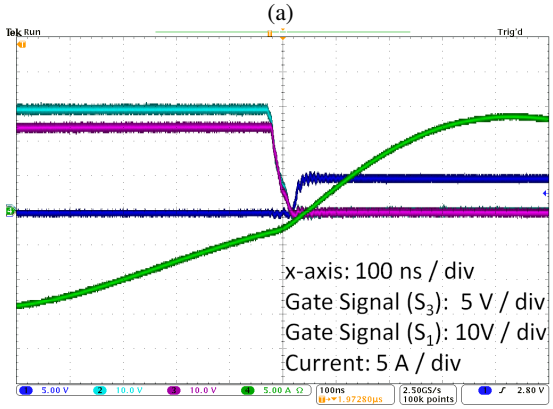

(b)

Fig. 12: Current and voltage waveforms of the RCN dc/dc converter when operated at an input voltage of 25 V, showing (a) turn-off transition and (b) turn-on transition. (1-blue) Gate voltage of switch S_3, (2-turquoise) gate voltage of switch S_1, (3-magenta) drain-source voltage of switch S_3 and (4-green) current through inductor of the matching network. Zero-voltage and near-zero-current switching is realized.

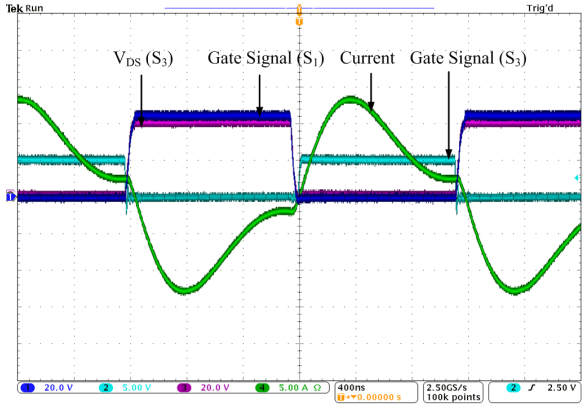

Fig. 13: Current and voltage waveforms of the RCN dc/dc converter when operated at an input voltage of 40 V: (1-blue) gate voltage of switch S_1, (2-turquoise) gate voltage of switch S_3, (3-magenta) drain-source voltage of switch S_3 and (4-green) current through inductor of the matching network.

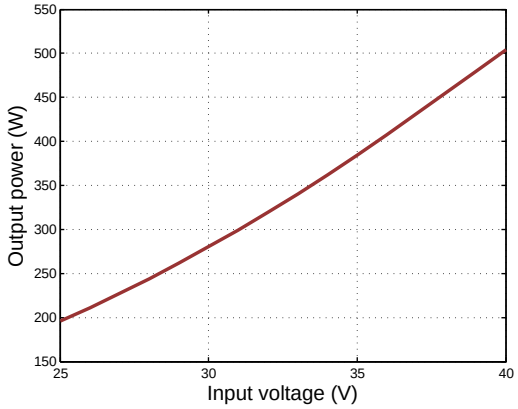

Fig. 14: Instantaneous output power with input voltage variation at fixed switching frequency of 500 kHz.

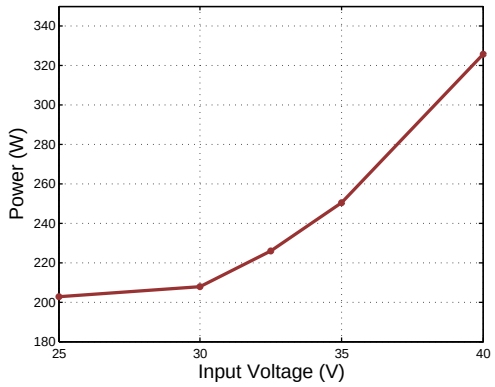

(a)

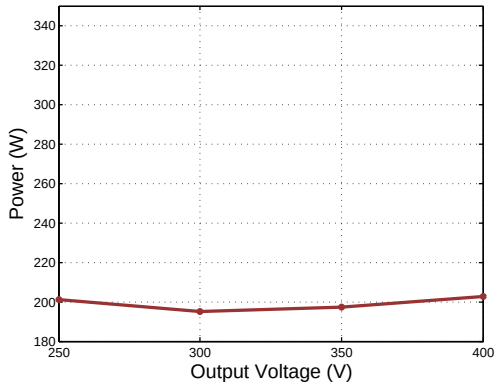

(b)

Fig. 15: Output power of the RCN dc/dc converter with (a) input voltage variation and (b) output voltage variation. The output power can be controlled below the levels indicated though on-off control. Note the effectiveness of the RCN in suppressing the effects of output voltage variation on the operation (output power) of the converter.

The efficiency of the RCN dc/dc converter was also measured across variations in input voltage, output voltage and output power. The measured efficiency of the converter as a function of input voltage is plotted in Fig. 17. The converter maintains efficiency above 95% across the full range of input voltage. The efficiency of the converter increases from 95% to 95.6% as input voltage increases from 25 V to 40 V. The efficiency of the converter as a function of output voltage is shown in Fig. 18. As the output voltage decreases from 400 V to 250 V, with input voltage held constant at 25 V, the efficiency of the converter drops from 95% to 93.7%. The lower efficiency at the lower output voltage is due to the larger currents flowing through the output stages of the converter.

The loss mechanisms in this prototype converter were estimated using equations provided in the appendix and data from component datasheets. Figure 19 shows the loss break down of the converter for an input voltage of 25 V, output voltage of 400 V and output power of 200 W. More than 50% of the loss is due to the magnetic elements, with the transformer causing the largest amount of loss. Semiconductor losses are the next largest category, followed by capacitor losses. Board trace losses (under 'other loss') can be reduced through appropriate board design.

The output power of the converter is controlled below its maximum value using on/off control at an on/off modulation frequency of 500 Hz. The output power is determined by the duty ratio of the modulation command waveform. A 100% duty ratio delivers maximum power (roughly 200 W at 25 V) and a 10% duty ratio corresponds to 10% of maximum power (roughly 20 W at 25 V). Fig. 20 shows the current flowing into the matching network (I_i in Fig. 2) and the voltage at the input of the matching network (V_i in Fig. 2) when the converter is operating with an on-off modulation duty ratio of 50% . Figure 21(a) shows these current and voltage waveforms when the converter turns on. It takes around 5 cycles for the current to achieve steady state. Figure 21(b) shows the same waveforms when the converter turns off. It takes around 30 cycles for the current to drop down to 10% of the peak current value. The total output capacitance is 126.4 μF, which reduces the peak-to-peak output voltage ripple to less than 2% over the entire power range. For the input, a 5000 μF capacitor was used. As the power supply

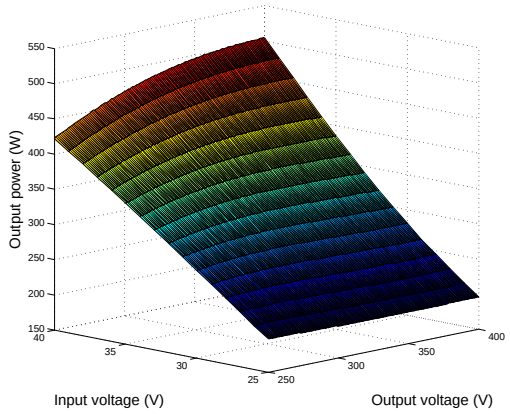

(a)

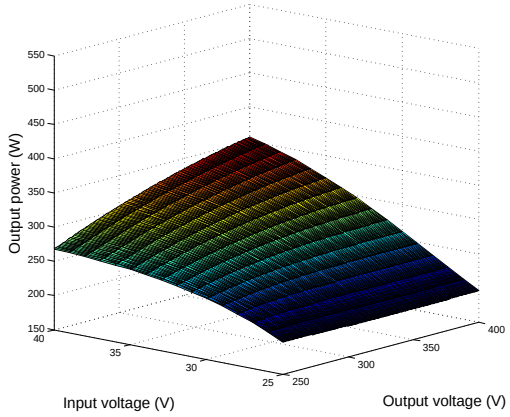

(b)

Fig. 16: Variation in output power of the RCN dc/dc converter as a function of input voltage and output voltage based on simulated results (a) under fixed (500 kHz) switching frequency operation, and (b) under narrow-range (425-500 kHz) switching frequency operation. While the resistance compression network substantially suppresses variations in output power with changes in output voltage, there is a significant variation in power with changes in input voltage. The narrow-band frequency control helps reduce this power output.

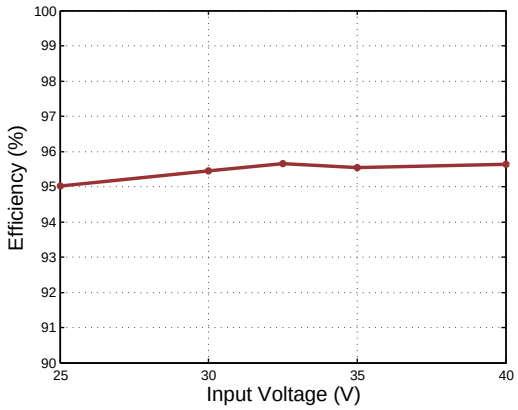

Fig. 17: Efficiency of the RCN dc/dc converter as the input voltage varies.

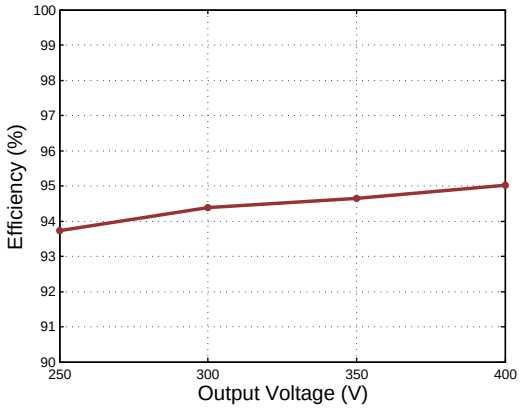

Fig. 18: Efficiency of the RCN dc/dc converter as the output voltage varies.

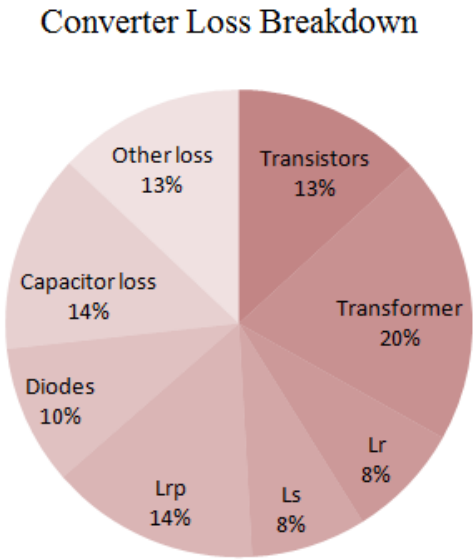

Fig. 19: Estimated breakdown of converter losses. The 'other loss' category includes board trace loss.

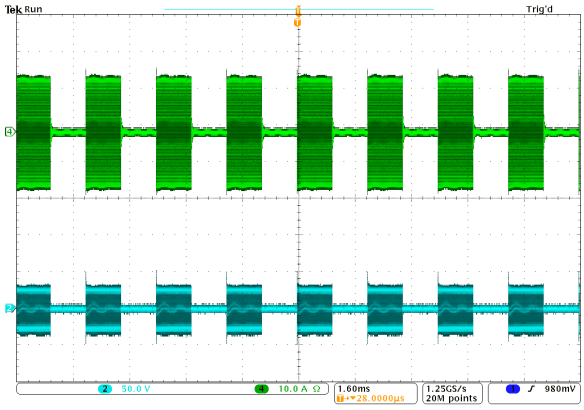

Fig. 20: (4-green) Input current and (2-turquoise) input voltage of the matching network with 50% duty ratio of on/off modulation.

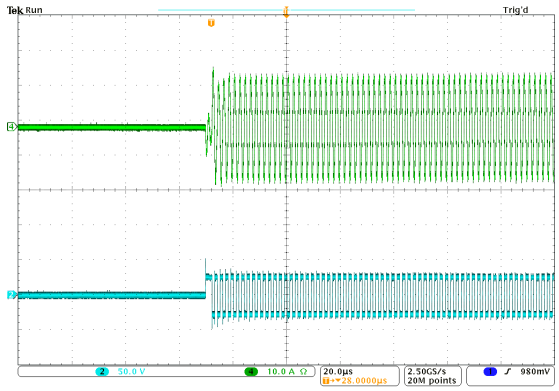

(a)

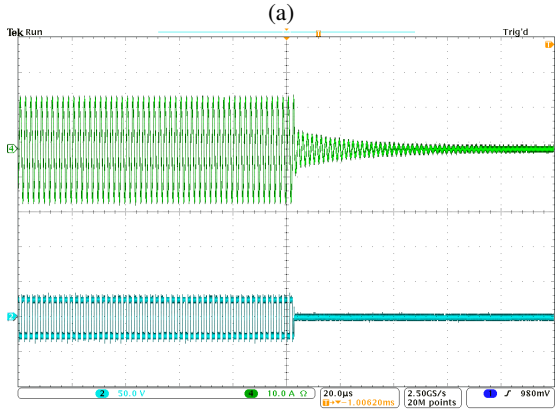

(b)

Fig. 21: (4-green) Input current and (2-turquoise) input voltage of the matching network with 50% duty ratio of on/off modulation at (a) turn-on and (b) turn-off.

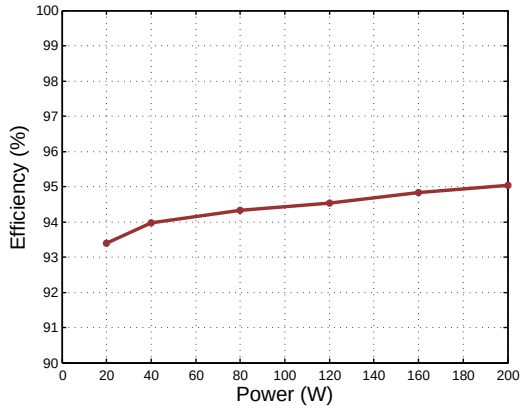

Fig. 22: Efficiency of the RCN dc/dc converter as the output power is varied using on/off control. This was measured with V_{in} = 25 V and V_{out} = 400 V.

driving the converter has very high output capacitance, less than 1% peak-to-peak ripple was observed. However, without the power supply's output capacitance, in the worst case, around 12% peak-to-peak ripple would be observed. This is in the range of ripple often allowed for PV systems (e.g., at 120 Hz or other frequencies) in order to provide information for maximum power point tracking. Reduced ripple is readily achieved by increasing input capacitance and/or increasing modulation frequency.

The efficiency of the converter as a function of output power is shown in Fig. 22. With input voltage of 25 V and output voltage of 400 V, the efficiency varies from 95% to 93.4% as output power is reduced from full load (200 W) to 10% of full load (20 W). These results demonstrate that the proposed RCN dc/dc converter can maintain ZVS and near ZCS operation and offer high efficiency across a wide input voltage, output voltage and output power range.

VI. Conclusion

This paper presents a new resonant dc/dc converter topology that uses a resistance compression network and a combination of on/off control and narrowband frequency control. The converter implementation provides galvanic isolation and enables large (greater than 1:10) voltage conversion ratios. The proposed converter achieves very high efficiency by maintaining ZVS and near ZCS over a wide input voltage, output voltage and power range. The experimental results from a 200 W prototype show that the converter maintains an efficiency of over 95% across its entire 25-40 V input voltage range at the designed output voltage of 400 V; an efficiency of over 93.7% as output voltage is reduced down to 250 V; and an efficiency of over 93.4% even as output power is reduced to 20 W. This demonstrates the effectiveness of the approach.

Acknowledgment

The authors wish to acknowledge the financial support received from the Masdar Institute for this project.

Appendix

Loss Estimation

This appendix provides the equations used to estimate the loss breakdown in the RCN converter presented in section V. As the transistors turn on under zero voltage their turn-on loss is negligible. Hence, the losses in the transistors are mainly conduction losses and turn-off losses. The conduction losses are estimated using the RMS current through each device and its on-state resistance. The turn-off losses are estimated assuming that the current through the transistors decreases linearly to zero when the device is switched off. Hence, the current through the transistor's output capacitance increases linearly resulting in a quadratic rise of voltage across the device. This overlap of current and voltage during the turn-off transition causes the loss. Thus the losses in a transistor are given by:

$$P_{tran} = I_{rms}^2 R_{ds-on} + \frac{I_{off}^2 t_f^2 f}{24 C_{oss}}. \quad (7)$$

Where I_{rms} is the RMS current through the transistor, R_{ds-on} is its on-state resistance, I_{off} is the current through the transistor at the instant when it is turned off, t_f is the fall-time of the current, f is the switching frequency and C_{oss} is the output capacitance of the transistor.

The diode loss is given by:

TABLE III: Parameter values of 3F3 material to calculate the power loss density.

Parameter	Value
C_m	2×10^{-5}
x	1.8
y	2.5
c_{t_1}	1.05×10^{-2}
c_{t_2}	0.77×10^{-4}

$$P_{diode} = I_{rms-d}^2 R_T + I_{avg-d} V_T, \tag{8}$$

where I_{rms-d} is the RMS current through the diode, R_T is its on-state resistance, I_{avg-d} is its average current, and V_T is its on-state voltage drop.

Losses in the magnetic components are comprised of the core losses and winding losses. The core losses are estimated as

$$P_{core} = C_m f^x B_{max}^y V (c_{t_0} - c_{t_1} T + c_{t_2} T^2), \tag{9}$$

C_m, x, y, c_{t_0}, c_{t_1}, and c_{t_2} are parameters found by curve fitting the measured power loss data [24] and are given in Table III. Here B_{max} is the maximum flux density through the core, V is its effective volume, and T is the core temperature. The winding losses in the case of litz wire are estimated using:

$$P_{cu-wire} = I_{rms-w}^2 R_{dc} F_r, \tag{10}$$

where I_{rms-w} is the RMS current through the wire, R_{dc} is the dc resistance of the wire and F_r is a factor that relates the dc losses to the ac losses assuming the current is sinusoidal [25]. The winding losses in the case of copper foil are estimated using:

$$P_{cu-foil} = I_{rms-f}^2 R_{dc} \frac{d}{\delta}, \tag{11}$$

where $I_{rms-foil}$ is the RMS current through the foil, d is the width of the copper foil and δ is the skin-depth.

Finally, capacitor losses are estimated using:

$$P_{cap} = I_{rms-c}^2 R_{ESR}, \tag{12}$$

where I_{rms-c} is the RMS current through the capacitor and R_{ESR} is its equivalent series resistance (ESR).

REFERENCES

[1] S. M. Chen, T. J. Liang, L. S. Yang, and J. F. Chen, "A Cascaded High Step-up dc/dc Converter with Single Switch for Microsource Applications," *IEEE Transactions on Power Electronics*, vol. 26, no. 4, pp. 11461153, Apr. 2011.

[2] S. V. Araujo, R. P. Torrico-Bascope and G. V. Torrico-Bascope, "Highly Efficient High Step-Up Converter for Fuel-Cell Power Processing Based on Three-State Commutation Cell," *IEEE Transactions Industrial Electronics*, vol. 57, no. 6, pp.1987-1997, Jun. 2010.

[3] Q. Zhao and F. C. Lee, "High-efficiency, high step-up dcdc converters," *IEEE Transactions on Power Electronics,* vol. 18, no. 1, pp. 6573, Jan. 2003.

[4] B. York, W. Yu, J. S. Lai, "An Integrated Boost Resonant Converter for Photovoltaic Applications," *IEEE Transactions on Power Electronics* , vol.28, no.3, pp.1199-1207, Mar. 2013

[5] J. S. Lai, "Power Conditioning Circuit Topologies," *IEEE Industrial Electronics Magazine*, pp. 24-34, Jun. 2009.

[6] Q. Li and P. Wolfs, "A Review of the Single-Phase Photovoltaic Module Integrated Converter Topologies with Three Different DC Link Configurations," *IEEE Transactions on Power Electronics*, vol. 23, no. 3, pp. 1320-1333, May 2008.

[7] R. L. Steigerwald, "High-Frequency Resonant Transistor DC-DC Converters," *IEEE Transactions on Industrial Electronics*, vol. IE-31, no. 2, pp. 181-191, May 1984.

[8] R. L. Steigerwald, "A Comparison of Half-Bridge Resonant Converter Topologies," *IEEE Transactions on Power Electronics*, vol. 3, no. 2, pp. 174-182, Apr. 1988.

[9] B. Sanzhong, Z. Pantic,S. Lukic, "A Comparison Study of Control Strategies for ZVS Resonant Converters," in Proc. *36th Annual Conference on IEEE Industrial Electronics Society*, Nov. 2010.

[10] R. T. H. Li, M. F. Vancu, F. Canales, D. Aggeler, "High performance dc-dc converter for wide voltage range operation," *7th International Power Electronics and Motion Control Conference (IPEMC)*, vol. 2, pp. 1151-1158, Jun. 2012

[11] J. P. Vandelac and P. D. Ziogas, "A DC to DC PWM Series Resonant Converter Operated at Resonant Frequency," *IEEE Transactions on Industrial Electronics*, vol. 35, no. 3, pp. 451-460, Aug. 1988.

[12] P. K. Jain, A. St-Martin and G. Edwards, "Asymmetrical Pulse-Width-Modulated Resonant DC/DC Converter Topologies," *IEEE Transactions on Power Electronics*, vol. 11, no. 3, pp. 413-422, May 1996.

[13] Y. S. Lee and Y. C. Cheng, "A 580 kHz Switching Regulator Using On-Off Control," *Journal of the Institution of Electronic and Radio Engineers*, vol. 57, no. 5, pp. 221-226, September-Oct. 1987.

[14] W. Inam, K. K. Afridi and D. J. Perreault, "High Efficiency Resonant dc/dc Converter Utilizing a Resistance Compression Network," in Proc. *IEEE Applied Power Electronics Conference and Exposition (APEC)*, Mar. 2013.

[15] Y. Han, O. Leitermann, D. A. Jackson, J. M. Rivas, and D. J. Perreault, "Resistance Compression Networks for Radio-Frequency Power Conversion," *IEEE Transactions on Power Electronics*, vol. 22, no. 1, pp. 41-53, Jan. 2007.

[16] P. A. Godoy, D. J. Perreault and J. L. Dawson, "Outphasing Energy Recovery Amplifier With Resistance Compression for Improved Efficiency," *IEEE Transactions on Microwave Theory and Techniques*, vol. 57, no. 12, pp. 2895-2906, Dec. 2009.

[17] Y. Han and D. J. Perreault, "Analysis and Design of High Efficiency Matching Networks," *IEEE Transactions on Power Electronics*, vol. 21, no. 5, pp. 1484-1491, Sep. 2006.

[18] J. M. Rivas, R. S. Wahby, J. S. Shafran, D. J. Perreault, "New Architectures for Radio-Frequency DCDC Power Conversion," *IEEE Transactions on Power Electronics* , vol. 21, no. 2, pp. 380-393, Mar. 2006.

[19] R. C. N. Pilawa-Podgurski, A. D. Sagneri, J. M. Rivas, D. I. Anderson, D. J. Perreault, "Very-High-Frequency Resonant Boost Converters," *IEEE Transactions on Power Electronics*, vol. 24, no. 6, pp. 1654-1665, Jun. 2009.

[20] J. M. Rivas, O. Leitermann, Y. Han, D. J. Perreault, "A Very High Frequency DCDC Converter Based on a Class ϕ_2 Resonant Inverter," *IEEE Transactions on Power Electronics*, vol. 26, no. 10, pp. 2980-2992, Oct. 2011.

[21] J. Hu, A. D. Sagneri, J. M. Rivas, Y. Han, S. M. Davis, and D. J. Perreault, "High-Frequency Resonant SEPIC Converter with Wide Input and Output Voltage Ranges," *IEEE Transactions on Power Electronics*, vol. 27, no. 1, pp. 189-200, Jan. 2012

[22] W. Inam, *High Efficiency Resonant dc/dc Converter for Solar Power Applications*, SM Thesis, Dept. of EECS, Massachusetts Institute of Technology, Cambridge, MA, Feb. 2013.

[23] D. Tian, L. R. Carley and D. S. Ricketts, "Frequency scaling of power reclamation networks in outphasing PA architectures," in Proc. *IEEE International Symposium on Circuits and Systems (ISCAS)*, May 2012.

[24] Ferroxocube Application Note, "Design of Planar Power Transformer", May 1997.

[25] C. R. Sullivan, "Optimal Choice for number of Strands in a Litz-Wire Transformer Winding," *IEEE Transactions on Power Electronics*, vol. 14, no. 2, pp. 283-291, Mar. 1999.